Creating Stiff, Tough, and Functional Hydrogel Composites with Low Melting Point Alloys

By *Riku Takahashi[1], Tao Lin Sun[2,3], Yoshiyuki Saruwatari[4], Takayuki Kurokawa[2,3], Daniel R. King[2,3]* & Jian Ping Gong[2,3]**

[1] R. Takahashi
Graduate School of Life Science, Hokkaido University, Sapporo 001-0021, Japan.

[2] Dr. T. L. Sun, Prof. T. Kurokawa, Dr. D. R. King, Prof. J. P. Gong,
Faculty of Advanced Life Science, Hokkaido University, Sapporo, 060-0810, Japan.

[3]Global Station for Soft Matter, Global Institution for Collaborative Research and Education, Hokkaido University, Sapporo, Japan.

[4] Y. Saruwatari
Osaka Organic Chemical Industry Ltd., Osaka 541-0052, Japan.

[*] Prof. J. P. Gong, Dr. D. R. King
Corresponding Authors. E-mail: (gong@sci.hokudai.ac.jp; dking@sci.hokudai.ac.jp)

Keywords: (Hydrogels, Composite Materials, Low Melting Point Alloys, Double Network Gels, Thermal Responsive Materials)

(Main Text)

Reinforcing hydrogels with a rigid scaffold is a promising method to greatly expand the mechanical and physical properties of hydrogels. One of the challenges of creating hydrogel composites is the significant stress that occurs due to swelling mismatch between the water-swollen hydrogel matrix and rigid skeleton in aqueous media. This stress can cause physical deformation such as wrinkling, buckling, or fracture, preventing the fabrication of robust composites. Here, we introduce a simple yet versatile method to create “macro-scale” hydrogel composites, by utilizing a rigid reinforcing phase that can relieve stress-induced deformation. A low melting point alloy (LMA) that can transform from a load-bearing solid state to a free-deformable liquid state at relatively low temperature was used as a reinforcing skeleton, which enabled us to release any swelling mismatch, regardless of the matrix swelling degree in liquid media. This design can generally provide hydrogels with hybridized functions, including excellent mechanical properties (stiffness comparable to metal and extremely high toughness), shape memory, and thermal healing, which are often difficult or

impossible to achieve with single-component hydrogel systems. Furthermore, this technique enables controlled electrochemical reactions and channel structure templating in hydrogel matrices. This work demonstrates a flexible pathway to develop hydrogel composites with unique functions, and may play an important role in the future design of soft robots, wearable electronics, and biocompatible functional materials.

Composite materials, consisting of a matrix and a reinforcing phase, can possess hybridized characteristics of each component, including physical, mechanical, and electrical properties.[1-3] This ability makes well-tuned composite materials uniquely desirable for specific applications in diverse fields, which may require properties that are unattainable with a single material. In particular, hydrogels exhibit a variety of properties that make them extremely useful as a matrix material, such as biocompatibility,[4,5] stimuli-responsiveness,[6] high flexibility,[7-9] controlled permeability,[10-12] antifouling,[13] low friction,[14] and optical clarity.[15,16] However, a serious problem has limited the use of hydrogels as a matrix material in combination with rigid reinforcements: stress-induced deformations can occur due to swelling mismatch between the hydrogel and the solid phase. In general, the volume of hydrogels can change dramatically from the as-prepared state by expelling water to, or absorbing water from, the environment.[17-19] This causes hydrogel-solid composites to undergo strain, resulting in surface creasing or bulk deformation, at best, and delamination or rupture, at worst.[20-22] To avoid or reduce deformation due to swelling mismatch, intense efforts have been devoted as follows: (1) relatively low-swelling hydrogels were used as a matrix to reduce the mismatch;[23-25] furthermore (2) geometrically compliant materials were incorporated that could deform by sliding (steel wool or glass-woven fibers), or stretching (nanometer scale reinforced gels),[23-26] and (3) mechanically compliant materials that could stretch (such as elastomers), were used as reinforcing materials to reduce the mismatch.[27] However, these approaches merely limit the impact of the induced stress, and are not fundamental solutions to swelling mismatch. As a result, the components of hydrogel-solid

composites have been highly selective. A universal strategy and practical methods for fabricating diverse hydrogel-based composites is strongly required for versatile applications.

To overcome such limitations, here, we report a new design concept and a simple fabrication method to prepare "macro-scale" hydrogel composites, consisting of a heterogeneous rigid phase within a soft hydrogel matrix, which can relieve swelling mismatch, preventing stress-induced physical deformation. A low melting point alloy (LMA) that can transform from a load-bearing solid state to a free-deformable liquid state at relatively low temperature (**Figure 1a, Figure S1**), was processed into a honeycomb-shaped grid (**Figure 1b**) and used as a reinforcement skeleton in the hydrogel-based composite. Due to the solid-liquid phase transition of LMAs, dramatic stiffness changes have been obtained in elastomer-based LMA composites.[28-30] Inspired by these composites, we attempted to release the stress caused by the swelling mismatch between the LMA and hydrogel by activating the solid-to-liquid phase transition.

To investigate whether we can relieve this mismatch in hydrogel composites, both deswelling (releases water from the as-prepared state) and swelling (absorbs water from the as-prepared state) hydrogel matrices were prepared from poly(2-ureidoethyl methacrylate)-co-(methacrylic acid) (PUMA) and polyacrylamide (PAAm) respectively, as model systems to produce hydrogel-LMA composites (**Figure 1c, Figure S2**). Combined with a honeycomb-shaped LMA skeleton as a reinforcing phase (**Figure 1b**), 50-mm-long and 10-mm-wide rectangle-shaped samples with a cross-sectional thickness of 2 mm were synthesized (**Figure 1d**). From the cross-section view in the inset of **Figure 1d**, the LMA skeleton was fixed nominally in the middle of the gel matrix (the insets show the PUMA composite, and the appearance of the PAAm composite was similar). After immersing the as-prepared composite gels in pure water for 1 week to allow the gels to reach the equilibrium state, both composite gels exhibited large stress-induced deformation due to the swelling mismatch between phases caused by the change in hydration of the hydrogel matrix as shown in **Figure 1e(i)**.

Specifically, the PUMA composite showed buckling and the PAAm composite showed surface creasing due to contraction of PUMA and swelling of PAAm in water, respectively. To release these stress-induced deformations, the samples were immersed in hot water (80ºC), causing the LMA to undergo a solid-liquid phase transition (the composition of the LMA used here is 32.5 % Bi, 51% In, and 16.5% Sn, resulting in a melting point of 60ºC). As expected, the LMA skeleton was transformed from the load-bearing solid state to the free-deformable liquid state (**Figure S1**). Thereafter, the swelling mismatch of the composites were spontaneously released, as shown by the squeezing out of LMA from the PUMA composite and the pore formation in the LMA of the PAAm composite (**Figure 1e(ii)**, **Movie S1 and Movie S2**). Note that the PAAm composite gel was subsequently refilled with additional LMA to recover a continuous LMA phase (**Figure S3**, **Movie S3**). As shown in **Figure 1f**, for both systems, there is little difference in volume change (from the initial to equilibrium state) for the composite and pristine gels, indicating that the LMA skeleton does not restrict the free swelling of the matrix hydrogel. From a detailed analysis, we observed that these size changes are isotropic (**Figure S4**). The volume fraction of LMA for both treated hydrogel composites was estimated as ~8.2% (compared to the total volume of the composites).

To confirm the reinforcing effect of the LMA phase in the composite hydrogels, uniaxial tensile tests were performed on the PUMA-LMA composite. Typical force-stretch curves of the PUMA composite, LMA honeycomb skeleton, and pristine PUMA gel are shown in **Figure 2a**. The PUMA composite exhibited much higher stiffness (~25 kNm^{-1}) than the pristine gel (~4 kNm^{-1}), similar to that of the LMA skeleton (~27 kNm^{-1}) (**Figure 2b**). However, the maximum stretch of the composite (~ 480%) was comparable to that of the pristine gel (~ 550%) and two orders of magnitude greater than that of the LMA skeleton (~ 6%). This is due to the unique fracture process of the composite, which results in a highly stretchable, yet stiff composite (**Movie S4**). As shown in the macrographs in **Figure 2a**, initially, the stress was concentrated in the stiff LMA skeleton, until it fractured. Then, the

stress was transferred to the soft hydrogel matrix that stretched until it reached a force that was comparable to the fracture force of the LMA skeleton (~16 N). After that, other regions of the LMA skeleton ruptured. Locally, the deformed regions of the gel were highly stretched, which enables high stress. However, rather than fracturing globally, the force caused the LMA skeleton to fracture, and this process continued many times. The composite hydrogel exhibits stretch values close to that of the pristine gel, but with force values near the fracture force of the LMA skeleton. This mechanical response mimics that of double network gels, where the LMA skeleton acts as the first network, imparting high modulus and breaking to dissipate energy, and the PUMA gel acts as the second network, stretching to maintain global integrity. The PUMA gel also dissipates viscoelastic energy, which is different from the second network of conventional double network hydrogels. As a result of the high stiffness and extensibility of the composite, the composite toughness was much higher than either single component (**Figure 2c**), representing a synergistic increase in mechanical properties.

It should be noted that the matrix component must possess a higher strength than the LMA skeleton to induce the multiple fracture process. This can be clearly seen in the behavior of the PAAm composite, in which the pristine PAAm gel is much weaker than the LMA skeleton (**Figure S5**). The composite also exhibited much higher stiffness (~37 kNm^{-1}) than the pristine gel (15 Nm^{-1}), similar to that of the LMA skeleton (~44 kNm^{-1}) **(Figure 2b**). However, due to the much lower fracture force of the PAAm hydrogel matrix (0.5 N) than the LMA skeleton (22 N), the matrix was unable to sustain the high force and fractured in one step, rather than the multiple fracture process seen in the PUMA hydrogel system (**Movie S5**). Thus, the toughness of the PAAm composite was as low as the LMA skeleton (**Figure 2c**).

The macroscopic double network-like phenomenon observed in the honeycomb-shaped PUMA-LMA composite bears many similarities to the recently reported fabric mesh-VHB tape composite system, reported by Hong and coworkers.[31] However, the force transmission between the two components of the composites are quite different for the two

systems. In the fabric mesh-VHB tape composite system, the force is transmitted by the adhesive interface, which requires very strong bonding between the two components. In the current composite system, in which the honeycomb-shaped LMA skeleton is embedded in the PUMA matrix, the force is transmitted through both mechanical interlocking and the adhesion between the PUMA matrix and the LMA skeleton. To justify this claim, the adhesion strength was characterized by performing a simple pull-out test on a rod of LMA embedded in the gels (**Figure S6**). The cross-sectional area of the LMA rods were the same as the LMA skeletons in the composites. The tests showed that the LMA rods could be pulled out from both of the two gels without breaking. As the length of the embedded rod increases, the pull-out force generated by the adhesion increases. However, in neither case was the adhesion sufficiently strong enough to cause fracture of the rods, even though the tested rod lengths were approximately four times greater than the honeycomb length dimension. In the case of the PUMA gel, the gel matrix largely deformed *prior to* sliding of the LMA rod, and the adhesion strength of the gel to LMA was estimated as ~0.3 MPa. Compared to the PUMA system, the adhesion of the PAAm hydrogel to LMA was very weak (~0.5 kPa) (**Figure S6**). These results indicate that the force transmission is mainly due to interlocking, not the adhesion, between the LMA skeleton and the gel matrix.

Utilizing a tough hydrogel, such as PUMA, as the matrix material is important towards developing extremely tough composite hydrogels, because it is capable of sustaining high load prior to fracture. The high strength of PUMA is due to the formation of hydrogen bonds between the polymer chains, as indicated by the deswelling of the PUMA hydrogel in water. Such hydrogen bonds serve as reversible sacrificial bonds to dissipate energy and causes toughening of the PUMA hydrogel based on the DN principle.[32,33] Accordingly, the PUMA-LMA composite have sacrificial bonds at two length scales: the molecular-scale hydrogen bonds and the macro-scale LMA skeleton.

The mechanical properties of LMA dramatically change at the melting point due to the solid-liquid phase transition.[28-30] Accordingly, the LMA composites exhibit a dramatic stiffness change in response to temperature. Utilizing the modulus difference between high and low temperature, the LMA composite gel can demonstrate repeatable shape memory as shown in **Figure 3a**. The composite gel could retain its shape due to the high stiffness of the internal LMA skeleton at room temperature (25ºC) (**Figure3a-i**). However, after immersing the composite into hot water (80ºC), the composite became flexible and returned to its as-prepared shape. The sample then became freely deformable (**Figure 3a-ii**), and when the composite was cooled while keeping a desired shape, the composite retained the new shape (**Figure 3a-iii**). When the shape-fixed composite was reheated above the melting point of the LMA, it spontaneously returned to the initial shape (**Figure 3a-iv**), due to the elastic restoring forces of the gel matrix. The ability to quickly change stiffness makes these hydrogel composites good shape memory materials, and opens up the possibility for use as variable stiffness actuators.[29]

To quantitatively characterize the mechanical response at low (25ºC) and high (80ºC) temperatures, the bending modulus and Young's modulus were measured by three-point bending tests and uniaxial tensile tests in cold (25ºC) and hot (80ºC) water, respectively (**Figure 3b**). At low temperature, the bending modulus and Young's modulus of the PUMA composite are approximately 30 and 100 times higher than those at high temperature, respectively. Also, the bending modulus and Young's modulus of the PAAm composite at low temperature are approximately 230 and 1000 times higher than those of the PAAm composite at high temperature. We should note that the difference between bending modulus and Young's modulus is due to the geometric anisotropy of the composite. Since the LMA skeleton is located nominally in the middle of the composite, during bending tests, it experiences smaller strain than the surrounding gel, biasing the composite modulus towards

that of the gel. Meanwhile, in the uniaxial tensile test, the strain is uniform across the cross-section of the sample, resulting in higher stiffness.

Beyond enhanced stiffness, toughness, and well-defined shape control, the composite hydrogels introduced here, possessing a macroscopic double network architecture, are capable of rigid first network healing, a process that conventional double network hydrogels cannot perform. When the composite samples with ruptured internal LMA skeletons were immersed in hot water (80ºC), the fragments of the internal LMA skeleton melted and re-formed (**Figure 3c-i and Figure 3c-ii**). After cooling the samples (25ºC), the LMA composites completely healed to the original state (**Figure 3c-iii and Figure 3c-iv**). To quantitatively evaluate the thermal healing efficiency, loading-unloading cyclic tests were performed with various cycle strains (0.5-2.5) and the mechanical response was measured. Typical load-unloading curves (cycle strain: 1.0) of the PUMA composite and the PUMA pristine gel are shown in **Figure 3d**. Three cycles of fracture and healing are shown. There were no significant differences between the stress-strain curves of the virgin samples and the thermally healed samples for both the pristine PUMA gel and the composite, showing that the healing efficiency, defined as the ratio between the hysteresis areas under the loading-unloading curve of the virgin sample and thermally healed sample, reached ~98%. It is expected that this cyclic healing process can be performed a significant number of times. Within this strain range, the dissipated energy (defined as the hysteresis area) of the composite gel (~ 0.95 MJ m^{-3}) was much higher than that of the pristine gel (~ 0.24 MJ m^{-3}), even after thermal healing. Similarly, the same analysis was performed with various cycle strains to investigate the thermal healing behavior (**Figure 3e**). Below a strain of 1.5, the healing efficiency of the composite was equivalent to the pristine gel. Above a strain of 2.0, the healing efficiency of the composite decreased compared to the pristine gel, because the gel matrix became damaged around the internal LMA skeleton during testing, and the liquid LMA could no longer reform sufficiently (**Figure S7**). In particular, above a cycle strain of 2.5, the gel

surrounding the LMA skeleton ruptured and thermal healing could not be performed due to leakage of the LMA. However, the dissipated energies in the healed composite above the cycle strain of 2.0 were still higher than that of the pristine gels. Therefore, this general method results in very tough hydrogel composites, with significant healing abilities. The healing efficiency likely can be improved through careful engineering of the reinforcing skeleton (changing geometry, matrix, and so on).[30]

Owing to the combination of different kinds of functional materials, the composite gels exhibit various unique characteristics in addition to the improved mechanical properties. For example, given the high electrical conductivity (2.4×10^6 Sm^{-1}) of LMA, similar to typical metals,[34] the LMA skeleton can serve as an electrode inside the hydrogel matrix to induce local electro-chemical reactions. **Figure 4a** demonstrates an example of electrolysis in a PAAm composite swollen in aqueous solution containing sodium chloride and phenolphthalein. After voltage was applied, hydroxide ions were generated around the LMA skeleton that was connected to the negative electrode of the power supply, which caused a chemical reaction with the phenolphthalein. Subsequently, a color-change was observed.[35] In addition to this, electro-polymerization can be performed at the interface between the LMA electrode and hydrogel matrix. When the hydrogel matrix contained sodium chloride and pyrrole, black polypyrrole was electro-chemically polymerized around the LMA skeleton that was connected to the positive electrode of the power supply (**Figure S8**, see **Supporting Information 1-9**). This electro-chemical reaction could be used to fabricate composites that have increased interfacial strength.[36,37]

In a contrasting approach, the LMA can be used as template to develop hydrogels with a programmed channel structure.[38-40] As shown in **Figure 4b**, by taking advantage of the solid-liquid phase transition of LMA, the internal LMA skeleton of the composite could be easily removed by air pressure in hot water, resulting in hydrogel fluidic devices. Such kind of hydrogel fluidic devices could be used for size excluded separation, controlled by the mesh

size of the gel matrix (currently: ~16 nm, see **Supporting Information 1-11**). For example, small dye molecules (~1 nm) could diffuse into the bulk of the hydrogel matrix (**Figure 4b-ii**), [41] while the large colloidal particles (~100 nm) could not (**Figure 4b-iii**). Given the high wettability of hydrogels, the hydrogel-based fluidic device showed strong capillary action to aqueous solutions (**Figure S9,** see **Supporting Information 1-12**). This result shows that the capillary action is precisely controlled by the geometry of the channels. Possessing the ability to rapid transport fluid over a long distance by capillary force, these hydrogel fluidic devices can serve as fast and efficient molecular filters or chemical reactors.[42,43]

In summary, macro-scale hydrogel composites based on low melting point alloys are prepared that represent a universal strategy to develop composites free of swelling-induced physical deformation. The resulting composites possess high stiffness, similar to the LMA phase. In particular, when the strength of the hydrogel matrix is higher than that of the internal LMA skeleton, the composites exhibit a synergistic increase in toughness, greater than either ~~neat~~ single component, based on the macro-scale double network effect. Additionally, by taking advantage of the solid-liquid phase transition of the LMA, dramatic stiffness changes can be triggered by a thermal stimulus, which simultaneously enables quick and highly efficient thermal healing properties. Furthermore, the combination of functional materials makes these materials uniquely designed for versatile functions such as performing electro-chemical reactions in the hydrogel matrix and creating channel structures in the hydrogel for fluidic devices. Utilizing low melting alloys in macroscopic composite hydrogels should enable the use of hydrogels in a wide range of field and applications that were previously incompatible for hydrogel materials.

(Experimental Section)
Experimental details are provided in the Supporting Information.

(Supporting Information)
Supporting Information is available online from Wiley Inter Science or from the author.

(Acknowledgement)
This research was financially supported by a Grant-in-Aid for Scientific Research (S) (No. 17H06144) and Grant-in-Aid for JSPS Fellows (No. 15J01078) from Japan Society for the Promotion of Science (JSPS). One of the authors, R.T., was supported by MEXT through Program for Leading Graduate Schools (Hokkaido University "Ambitious Leader's Program"). D.R.K. thanks the Hokkaido University Tenure-Track System for financial support.

Received: ((will be filled in by the editorial staff))
Revised: ((will be filled in by the editorial staff))
Published online: ((will be filled in by the editorial staff))

(References)

[1] U. G. K. Wegst, H. Bai, E. Saiz, A. P. Tomsia, R. O. Ritchie, *Nat. Mater.* **2014,** *14,* 23.

[2] X. Sun, H. Sun, H. Li, H. Peng, *Adv. Mater.* **2013,** *25,* 5153.

[3] B. C-K. Tee, C. Wang, R. Allen, Z. Bao, *Nat. Nanotechnol.* **2012,** *7,* 825.

[4] S. Hong, D. Sycks, H. F. Chan, S. Lin, G. P. Lopez, F. Guilak, K. W. Leong, X. Zhao, *Adv. Mater.* **2015,** *27,* 4035.

[5] P. Li, Y. F. Poon, W. Li, H.-Y. Zhu, S. H. Yeap, Y. Cao, X. Qi, C. Zhou, M. Lamrani, R. W. Beuerman, E.-T. Kang, Y. Mu, C. M. Li, M. W. Chang, S. S. J. Leong, M. B. Chan-Park, *Nat. Mater.* **2011,** *10,* 149.

[6] H. Guo, N. Sanson, D. Hourdet, A. Marcellan, *Adv. Mater.* **2016,** 28, 5857. b) X. Huang, Y. Sun, S. Soh, *Adv. Mater.* **2015,** *27,* 4062.

[7] K. Haraguchi, T. Takehisa, *Adv. Mater.* **2002,** *14,* 1121.

[8] J.-Y. Sun, X. Zhao, W. R. K. Illeperuma, O. Chaudhuri, K. H. Oh, D. J. Mooney, J. J. Vlassak, Z. Suo, *Nature* **2012,** *489,* 133.

[9] T. Sakai, T. Matsunaga, Y. Yamamoto, C. Ito, R. Yoshida, S. Suzuki, N. Sasaki, M. Shibayama, U. Chung, *Macromolecules* **2008,** *41,* 5379.

[10] N. Hirota, Y. Kumaki, T. Narita, J. P. Gong, Y. Osada, *J. Phys. Chem. B* **2000,** *104,* 9898.

[11] A. N. Peppas, J. Z. Hilt, A. Khademhosseini, R. Langer, *Adv. Mater.* **2006,** *18, 1345.*

[12] S. Lin, H. Yuk, T. Zhang, G. A. Parada, H. Koo, C. Yu, Z. Zhao, *Adv. Mater.* **2016,** *28,* 4497.

[13] I. Banerjee, R. C. Pangule, & R. S. Kane, *Adv. Mater.* **2011,** *23,* 690.

[14] J. P. Gong, T. Kurokawa, T. Narita, G. Kagata, Y. Okada, G. Nishimura & M. Kinjo, *J. Am. Chem. Soc.* **2001,** *123,* 5582.

[15] J. Franklin, A. Y. Wang, *Chem. Mater.* **2002,** *14,* 4487.

[16] H. Yuk, S. Lin, C. Ma, M. Takaffoli, N. X. Fang, X. Zhao, *Nat. Commun.***2017,** 8, 14230.

[17] A. B. Imran, K. Esaki, H. Gotoh, T. Seki, K. Ito, Y. Sakai, Y. Takeoka, *Nat. Commun.* **2014,** *5,* 5124.

[18] D. J. Beebe, J, S. Moore, J. M. Bauer, Q. Yu, R. H. Liu, C. Devadoss, B.-H. Jo, *Nature* **2000,** *404,* 588.

[19] T. L. Sun, T. Kurokawa, S. Kuroda, A. B. Ihsan, T. Akasaki, K. Sato, Md. A. Haque, T. Nakajima, J. P. Gong, *Nat. Mater.* **2013,** *12,* 932.

[20] T. Tanaka, S.-T. Sun, Y. Hirokawa, S. Katayama, J. Kucera, Y. Hirose & T. Amiya, *Nature* **1987,** *325,* 796.

[21] Zhang, X. C. L. Pint, M. H. Lee, B. E. Schubert, A. Jamshidi, K. Takei, H. Ko, A. Gillies, R. Bardhan, J. J. Urban, M. Wu, R. Fearing, Ali, Javey, *Nano Lett.* **2011,** 11, 3239.

[22] M. Y. Kim, B. Jung, J.-H. Park, *Biomaterials* **2012,** *33,* 668.

[23] D. R. King, T. L. Sun, Y. Huang, T. Kurokawa, T. Nonoyama, A. J. Crosby & J. P, Gong, *Mater. Horiz.* **2015,** *2,* 584.

[24] Y. Huang, D. R. King, T. L. Sun, T. Nonoyama, T. Kurokawa, T. Nakajima, J. P. Gong, *Adv. Funct. Mater.* **2017,** *27,* 1605250.

[25] W. R. K. Illeperuma, J.-Y. Sun, Z. Suo & J. J. Vlassak, *Extreme Mechanics Lett.* **2014,** *1,* 90.

[26] K. Tonsomboon, A. L. Butcher & M. L. Oyen, *Materials Science & Engineering C.* **2017,** *72,* 220.

[27] H. Yuk, T. Zhang, G. A. Parada, X. Liu, X. Zhao, *Nature Commun.* **2016,** *7,* 12028.

[28] E. B. Schubert & D. Floreano, *RSC Advances* **2013,** *3,* 24671.

[29] I. M. V. Meerbeek, B. C. M. Murray, J. W. Kim, S. S. Robinson, P. X. Zou, M. N. Silbertein & R. F. Shepherd, *Adv. Mater.* **2016,** *28,* 2801.

[30] A. Tonazzini, S. Mintchev, B. Schubert, B. Mazzolai, J. Shintake & D. Floreano, *Adv. Mater.* **2016,** 28, 10142.

[31] X. Feng, Z. Ma, J. V. MacArthur, C. Giuffre, A. Bastawros & W. Hong, *Soft Matter* **2016,** *12,* 8999.

[32] J. P. Gong, *Soft Matter* **2010,** *6,* 2583.

[33] J. P. Gong, Y. Katsuyama, T. Kurokawa, Y. Osada, *Adv. Mater.* **2003,** *15,* 1155.

[34] A. Ainla, S. Xu, N. Sanchez, G. D. M. Jeffries, & A. Jesorka, *Lab Chip* **2012,** *12,* 4605.

[35] J. Tian, T. Arbatan, X. Li, & W. Shen, *Chem. Comm.* **2010,** *46,* 4734.

[36] M. Sasaki, B. C. Karikkineth, K. Nagamine, H. Kaji, K. Torimitsu & M. Nishizawa, *Adv. Healthc. Mater.* **2014,** *11,* 1919.

[37] Y. Gao, S. J. Song, S. Li, C. Elowsky, Y. Zhou, S. Ducharme, Y. M. Chen, Q. Zhou & L. Tan, *Nat. Commun.* **2016,** *7,* 12316.

[38] D. P. Parekh, C. Ladd, L. Panich, L. Moussa, M. D. Dickey, *Lab Chip* **2016,** *16,* 1812.

[39] A. Fassler, C. Majidi, *Lab Chip* **2013,** *13,* 4442.

[40] M. D. Dickey, *ACS App;. Mater. Interfaces* **2014,** *6,* 18369.

[41] H. Feil, Y. H. Bae, J. Feijen, S. W. Kim, *J. Membrane Sci.* **1991,** *64,* 283.

[42] S. Han, T. Wang, & B. Li, *J. Appl. Poly. Sci.* **2017,** *134,* 1.

[43] R. K. Garg, R. C. Rennert, D. Duscher, M. Sorkin, R. Kosaraju, L. J. Auerbach, J. Lennon, M. T. Chung, L. Paik, J. Nimpf, N. Rajadas, M. T. Longaker & G. C. Gurtner, *Stem Cells Trans. Med.* **2014,** *3,* 1079.

(Figures)

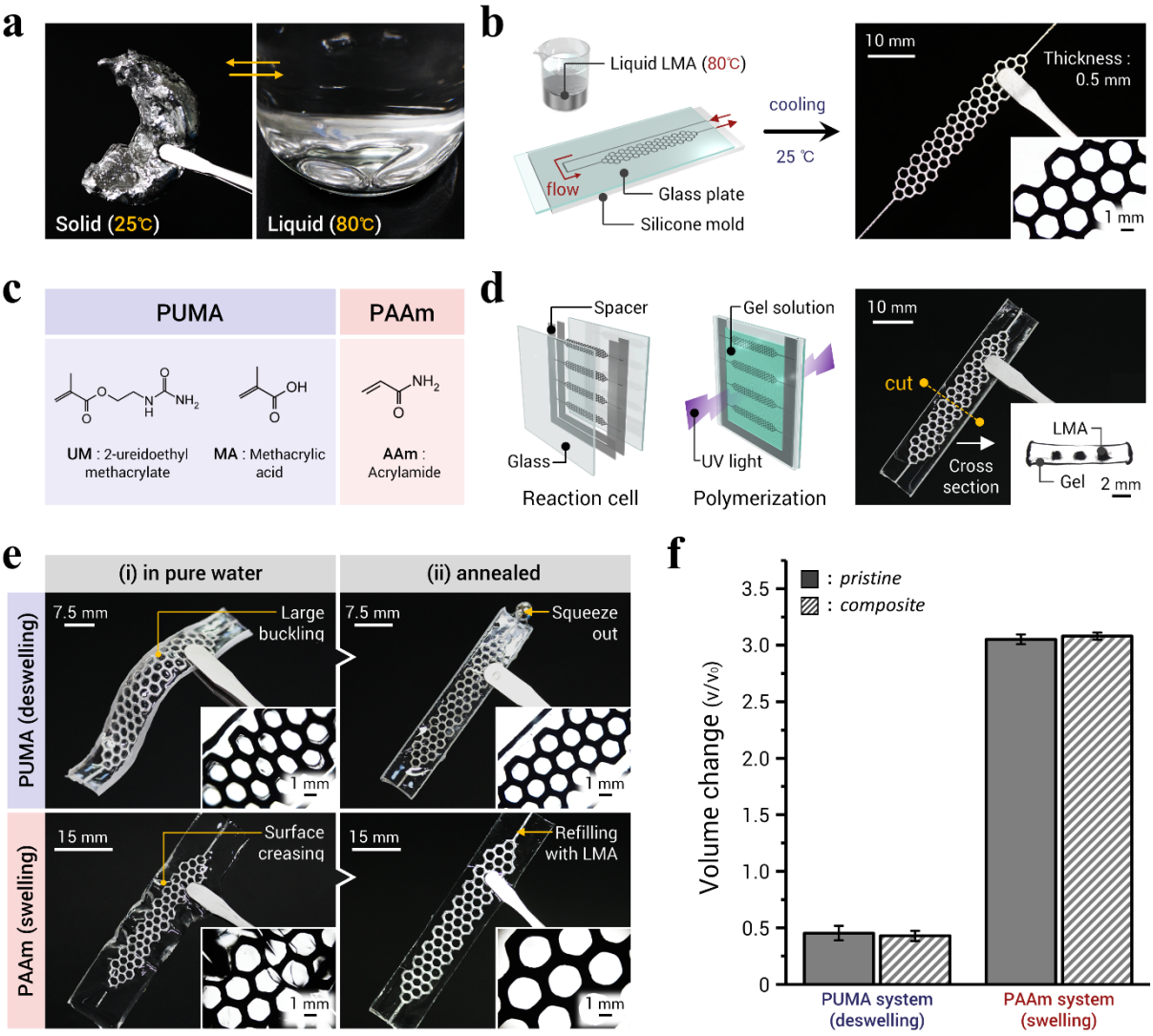

Figure 1. Fabrication of hydrogel-LMA composites without swelling mismatch. (a) Solid-liquid phase transition of the low melting point alloy (LMA); the composition of the LMA is 32.5 % Bi, 51% In, and 16.5% Sn. (b) Schematic illustration of the fabrication process of honeycomb-shaped LMA skeletons from a silicone mold and photograph of the resulting LMA skeleton. The inset image is an optical micrograph of the LMA skeleton observed from the top. (c) Chemical structures of the monomers for PUMA (light blue) and PAAm (pink) systems. (d) Schematic illustration of the fabrication process of the composites and photograph of an as-prepared PUMA composite. The inset image is an optical micrograph of the cross-section. The appearance of the as-prepared PAAm composite is similar to the as-prepared PUMA composite. (e) Photographs of the composites equilibrated in pure water (i) before and (ii) after the thermal annealing treatment. Due to shrinkage (or swelling) of the PUMA (or PAAm) in water, which induces a large mismatch between the gel and LMA solid skeleton, large buckling (or surface creasing) was observed. After thermal annealing by immersing the samples in 80°C water, the swelling mismatch was spontaneously released due to melting of the LMA. Inset images are optical micrographs observed from the top direction. (f)Volume changes of the pristine gels and composite gels, relative to the as-prepared state, after equilibrium in water. Both deswelling and swelling hydrogel systems exhibited the same volume changes between the pristine gel and the composite. Each measurement was performed 3-5 times. Error bars represent standard deviation.

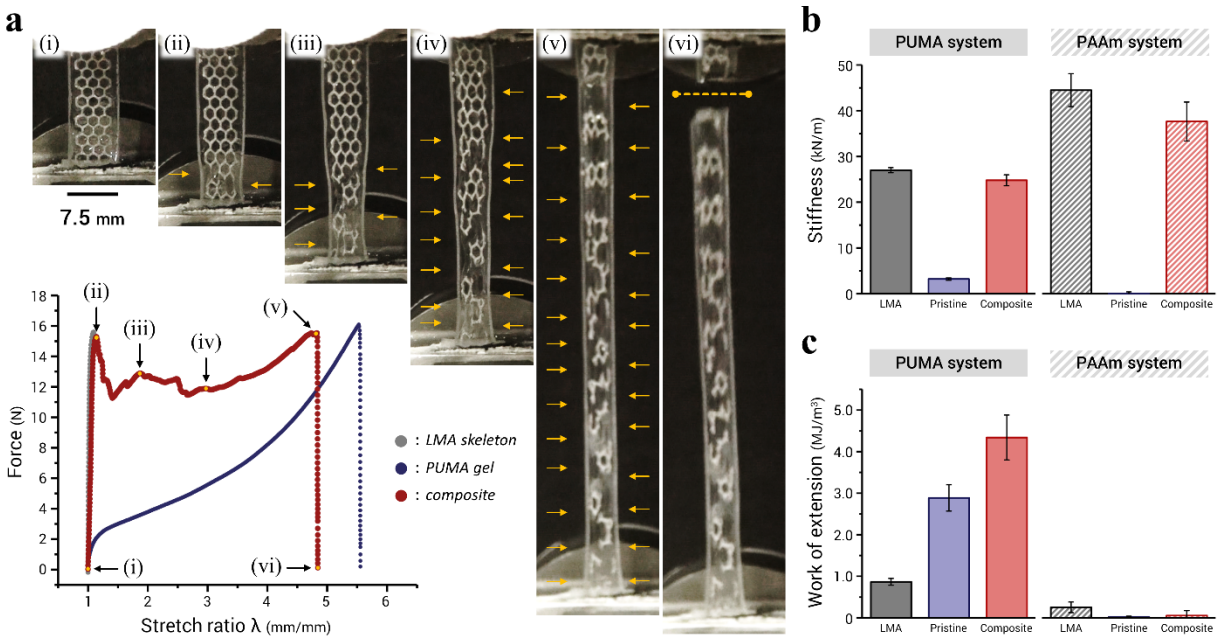

Figure 2. Mechanical properties of PUMA-LMA composites (a) Force-stretch curves of a honeycomb mesh LMA skeleton (grey), a pristine PUMA gel (navy) and their composite (wine). The insets (i)-(vi) represent snapshots of the composite sample at the corresponding stretch shown in the loading curves. Initially, the force of the composite rapidly increased and the LMA skeleton broke at a force comparable to that of the LMA skeleton (i-ii). During further stretching of the sample (ii-v), multiple fractures of the LMA skeleton were observed (inset arrows indicate fracture points), while the hydrogel matrix maintained global integrity. As a result, bulk fracture did not occur. Finally, the hydrogel matrix ruptured at the position shown by the dashed line (vi). (b) Stiffness of each component and the composite in the respective system. (c) Strain energy density (area below the stress-strain curve) of each component and composite in the respective system. Each mechanical test was performed 3-5 times. Error bars represent standard deviation.

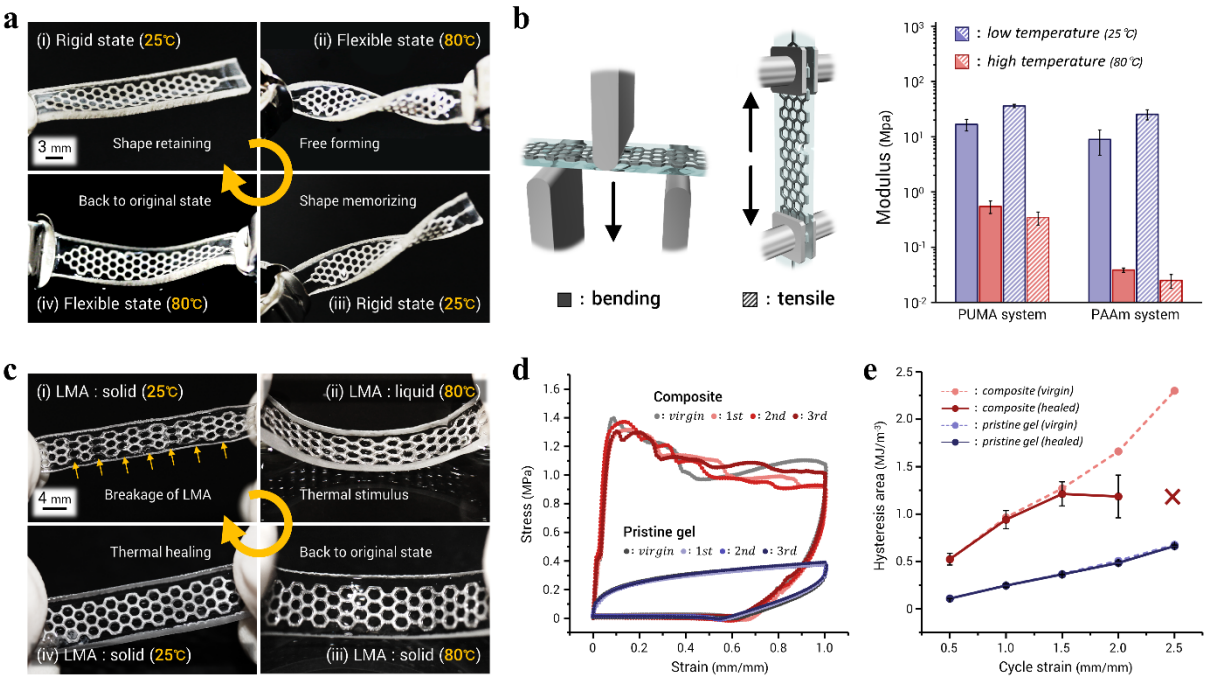

Figure 3. Thermal response and thermal healing of PUMA-LMA composites. (a) Demonstration of shape memory based on the solid-liquid phase transition of the LMA skeleton. (b) Bending (solid shade) and tensile (hashed) moduli of the composite at low (25ºC, blue) and high (80ºC, red) temperature. (c) Demonstration of thermal healing ability at a strain ratio of approximately 1.5. Inset arrows in (i) represent the broken points of the internal LMA skeleton. (d) Cyclic test curves of composite and pristine PUMA gels. (e) Mechanical hysteresis loss during loading and unloading testing at various strains (0.5-2.5). The data for the healed composite at a strain of 2.5 was not measured due to damage of the sample during the first cycle. Each measurement was performed 3-7 times. Error bars represent standard deviation, and are smaller than the marker unless explicitly shown.

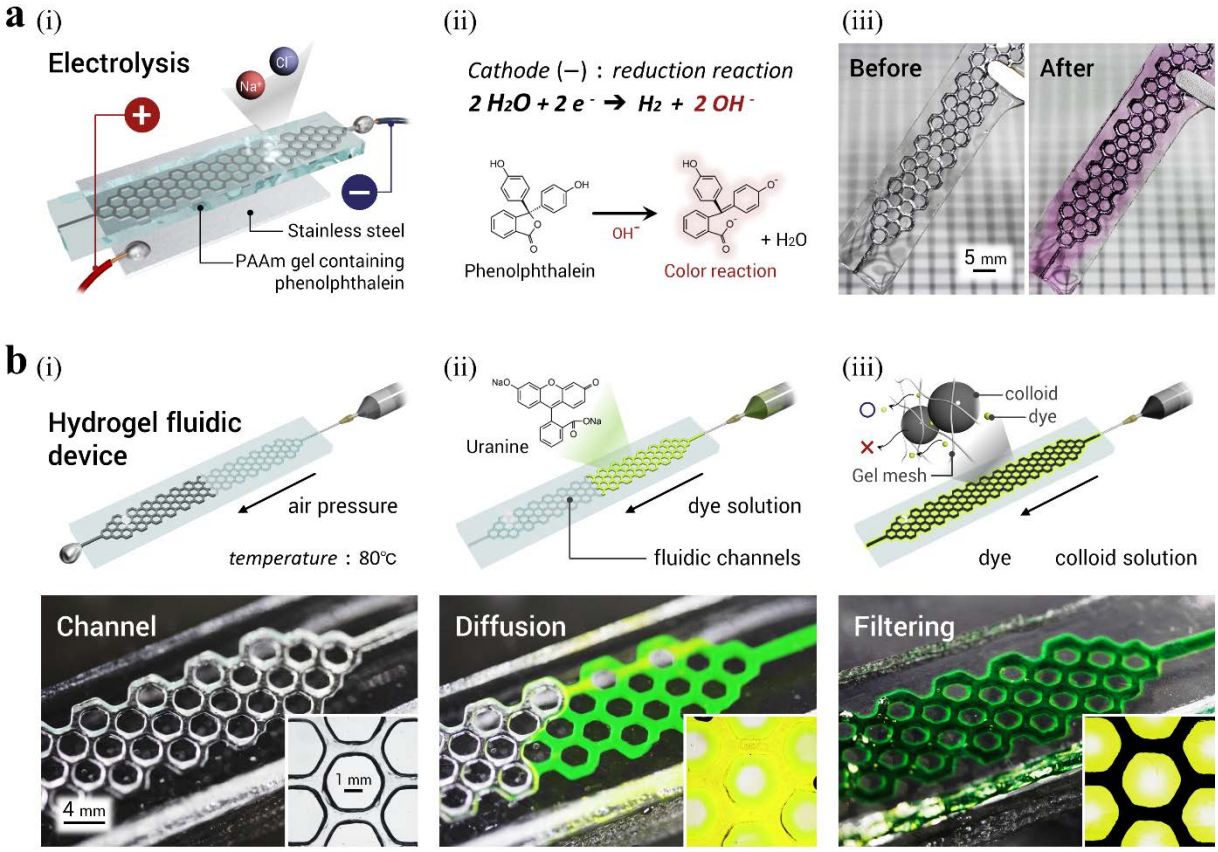

Figure 4. Unique applications of LMA-based macro-scale hydrogel composites. (a) Demonstration of electro-reduction in the hydrogel matrix for the composite swollen with NaCl aqueous solution (0.15 M). (i) By connecting the LMA skeleton to the negative electrode and the gel to the positive electrode of a 3V power supply, (ii) a reduction reaction was induced and hydroxide ions were generated around the LMA skeleton. (iii) When the hydrogel matrix contained phenolphthalein, a color response was observed after electrolysis due to the reaction between the phenolphthalein and the hydroxide ions. (b) Demonstration of a PAAm hydrogel fluidic device utilizing the LMA skeleton as a channel template; (i) photograph and optical micrograph (inset) of the channel structure, (ii) demonstration of hydrogel fluidic channels by diffusion of green dye molecules (Uranine) into the hydrogel matrix (inset picture), (iii) hydrogel filtration of black colloidal particles (Indian ink) from a mixture with green dye (Uranine) when passed through the hydrogel channels. The upper row are illustrations to show channel fabrication (i), dye diffusion (ii), and filtration (iii).